encit 2020

ABCM Associação Brasileira de Engenharia e Ciências Mecânicas

18th Brazilian Congress of Thermal Sciences and Engineering
November 16–20, 2020 (Online)

ENC-2020-0067
AN INERTIAL AIR-STANDARD FINITE-TIME HEAT ADDITION OTTO ENGINE MODEL

Filipe Macedo Moreira
Christian Naaktgeboren, Ph.D.
Universidade Tecnológica Federal do Paraná, Câmpus Guarapuava
filipemoreira@alunos.utfpr.edu.br
NaaktgeborenC@utfpr.edu.br

Abstract. *This work proposes a novel, multi-disciplinary, coupled, dynamic–thermodynamic, inertial air-standard model for spark-ignited Otto engines that takes into account effects as (i) finite-time heat release, (ii) crank-rod mechanism geometry, basic engine dimensions and operating parameters, as well as (iii) piston, rod, crankshaft, and flywheel inertias. The present model is a two-way coupling between models from the somewhat recent literature, one being predominantly (i) thermodynamic and the other (ii) dynamic in their natures, with the necessary adjustments. The thermodynamic model captures non-trivial, simultaneous heat and work interactions during non-instantaneous heat-releasing processes, while the dynamic model accounts for variable engine angular velocity, as well as translation and rotation inertia of key components, which are taken as rigid bodies. The coupled model herein proposed is able to predict instantaneous and time-averaged crankshaft torque, angular speed and engine power, in terms of several key engine design and operating parameters. Moreover, the model can be suited for teaching in advanced undergraduate and graduate courses.*

Keywords: *Inertial, finite-time, heat addition, Otto engine, iFTHA, variable speed, two-way coupling, dynamic-thermodynamic model.*

1. INTRODUCTION

Equilibrium thermodynamic models of internal combustion engines can be as simple as the ideal, air-standard Otto cycle taught in engineering thermodynamics textbooks (Çengel and Boles, 2013; Borgnakke and Sonntag, 2009), or incorporate effects such as combustion (Curto-Risso *et al.*, 2008); chemical equilibrium, crank-rod mechanism and engine dimensions and operating parameters (Brunetti, 2012; Martins, 2013); friction and heat-transfer irreversibilities (Rubin, 1979; Salamon and Nitzan, 1981; Mozurkewich and Berry, 1982; Hernandez *et al.*, 1995; Liley, 1999; Özcan, 2011; Ebrahimi, 2014; Seddak and Liazid, 2017); as well as pressure-drop irreversibilities (Huleihil, 2011); as to provide progressively more accurate performance predictions.

On the one hand, such improvements quickly cause the resulting model to depart from pure-substance, internally reversible thermodynamics of the typical engineering undergraduate engineering curriculum; on the other hand, significant deviations to experimental results (Brunetti, 2012; Martins, 2013) seem to remain in improved models whenever the *instantaneous* heat release (or combustion) hypothesis is kept.

One can therefore argue that the removal of isochoric heating must be the first improvement to be done in an otherwise ideal model—that will cause the model to remain a pure-substance, internally reversible one—resulting in most prediction improvements per model complexity increase, before other effects—such as combustion, heat-transfer, and pressure-drop irreversibilities—are incorporated. Such a Finite-Time Heat Addition, FTHA, model has been published in a somewhat recent study (Naaktgeboren, 2017), which turned up as an easy-to-teach model that is able to reproduce some key features of experimental P–v diagrams.

A similar observation can be drawn from the evolution of dynamic engine models for load calculations (Horváth and Égert, 2015): simple textbook models assuming constant angular velocity and lumped components without rotation inertia (Norton, 2010; Brunetti, 2012) quickly incorporate mathematical complexity (Villalva, 2014), external tools (Barros, 2003), and even elasticity (de Souza Neves, 2010) while still keeping the crank angular velocity constant, which represents a one-way coupling with the thermodynamic model. There is, however, a model by Montazersadgh (2007) of rigid body, inertial components and variable angular velocity that is a more naturally suited, two-way coupled, dynamic model refinement to go along with a FTHA thermodynamic model.

This work presents a *two-way coupled* model between models of references (Naaktgeboren, 2017) and (Montazersadgh, 2007), with the necessary adjustments and some results. Further detailed model information can be found in (Moreira, 2019). Moreover, the model is believed to be suitable for teaching in advanced settings.

2. METHODOLOGY

2.1 Thermodynamic Modeling

Let engine piston-rod-crank mechanism parameters be crank radius R and clockwise-increasing position α, rod length L, piston diameter D; and operating parameters stroke $S = 2R$, top- and bottom-dead center volumes V_{min}, V_{max}, and clockwise-increasing operating angular speed $\omega \equiv \dot{\alpha}$, according to Fig. 1. Let $r = V_{max}/V_{min}$ be the engine compression ratio, $V_d = zV_{du} = z(V_{max} - V_{min})$ be the engine displaced volume, with z being the number of cylinders and $V_{du} = \pi S D^2/4$ the unit displacement volume.

Let further the piston position x, with $0 \leqslant x \leqslant S$, shown in Fig. 1. The $x(\alpha)$ relationship is known to be $x(\alpha) = L[1 - \sqrt{1 - (R\sin\alpha/L)^2}] + R(1 - \cos\alpha)$ (Brunetti, 2012). In the current model, the instantaneous system specific volume v is known at all times from the system mass m and instantaneous volume $V = V_{min} + (\pi D^4/4)x$.

In the coupled model, the four Otto cycle logical processes (Naaktgeboren, 2020) of (i) adiabatic compression, (ii) head addition, (iii) adiabatic expansion, and (iv) heat removal are *time*-discretized—meaning $t_{i+1} = t_i + \Delta t$, and $\alpha_{i+1} = \alpha_i + \omega_i \Delta t$—and uniformly modeled with local polytropic processes (Naaktgeboren, 2020) of const-(Pv^{n_i}), where $i \in \mathbb{Z}$ is the process index, while the logical heat addition process (ii) is allowed to occur in a finite time Δt_c; thus, no longer being isochoric. The logical heat removal process (iv) is kept isochoric in the classical FTHA (Naaktgeboren, 2017).

The energy balance for the i-th discrete process is

$$q_i + w_i = \Delta u_i = u_{i+1} - u_i, \tag{1}$$

where q_i and w_i are the heat and work transfers *to* the system during the process, while $u_{\mathsf{x}}, \mathsf{x} \in \{i, i+1\}$, are the system specific internal energies in the given state indices; the balance is solved for u_{i+1} by (i) modeling q_i and by (ii) iteratively solving for the discrete process polytropic exponent, n_i, which, in turn, determines w_i.

The heat release model that establishes all q_i's employs an auxiliary cumulative heat release function, $y(t)$, given by:

$$y(t^\star) = \begin{cases} 0, & \text{for } t^\star < t^\star_\theta, \\ g(t^\star), & \text{for } t^\star_\theta \leqslant t^\star < t^\star_\theta + \Delta t_c, \\ 1, & \text{for } t^\star_\theta + \Delta t_c \leqslant t^\star. \end{cases} \tag{2}$$

with the current cycle time $t^\star$ being a shifted time reset to zero at the beginning of each cycle. On Eq. (2), $g(t^\star)$ is the cumulative heat release function due to the combustion process, which can be obtained either from experiments or from the literature. One therefore models the process heat release as $q_i = q_{ent}\Delta y_i$, with $\Delta y_i = y(t^\star_{i+1}) - y(t^\star)$. The ignition time $t^\star_\theta$ is such that $\alpha(t^\star_\theta) = \theta$, holds true.

The iterative process on the j-th estimate of values $\{n, w\}_i^j$ and $\{u, T, P\}_{i+1}^j$ follows:

$$u_{i+1}^j = u_i + q_i + w_i^j, \quad \text{with} \tag{3}$$

$$w_i^j = \begin{cases} \frac{P_i v_i}{1-n_i^j} \cdot \left[1 - \left(\frac{v_i}{v_{i+1}}\right)^{n_i^j - 1}\right], & \text{for} \quad n_i^j \neq 1 \\ P_i \cdot v_i \cdot \ln\left(\frac{v_i}{v_{i+1}}\right), & \text{for} \quad n_i^j = 1 \end{cases} \tag{4}$$

$$T_{i+1}^j = f(u_{i+1}^j, c_v(T), v_{i+1}), \tag{5}$$

$$P_{i+1}^j = f(T_{i+1}^j, v_{i+1}), \quad \text{finally correcting for } n_i^j \text{ with} \tag{6}$$

$$n_i^{j+1} = \left(\log \frac{P_{i+1}^j}{P_i}\right) \Big/ \left(\log \frac{v_i}{v_{i+1}}\right). \tag{7}$$

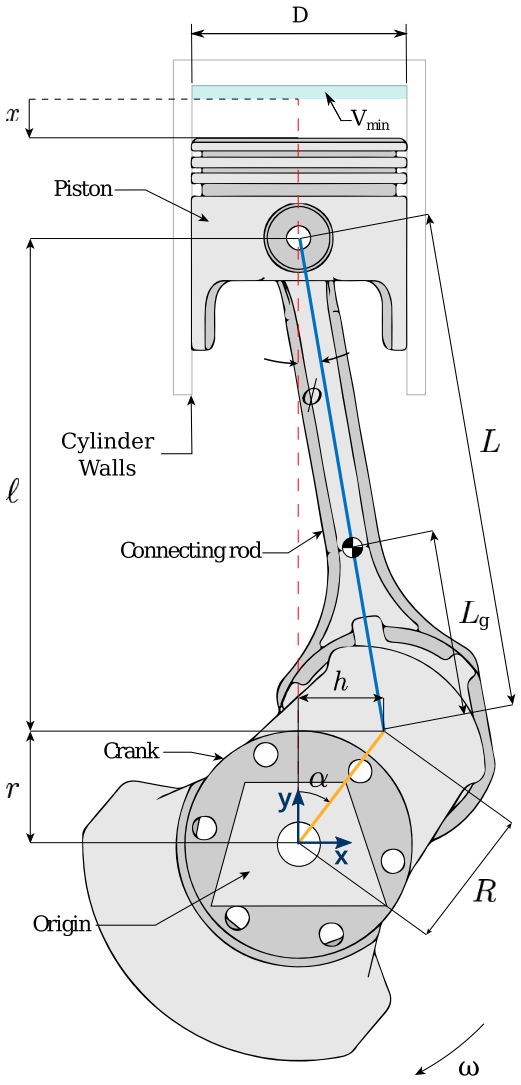

Figure 1. Model piston-rod-crank mechanism. Adapted from Tzortzinis (2015).

The specific volumes are taken from volume relations with respect to the piston position $x(\alpha(t))$, and initial system mass, which is estimated from initial (admission) conditions (P_0, T_0, V_0). Once j-convergence is achieved, state-$(i+1)$ is determined.

The pressure force in the piston head is the thermodynamic input on the dynamic model, described next, while variations in engine angular velocity, $\dot{\omega}$—which influences discrete values of $\alpha(t)$, $x(\alpha(t))$, and through it, specific volume variations—is the dynamic model input on the thermodynamic model; and thus, the two-way coupling in the model.

2.2 Dynamic Modeling

For the dynamic model, the reference coordinate system is the right-handed, Cartesian, ortho-normal and static one, with the **x**- and **y**-axes shown in dark blue on Fig. 1. Fundamental hypotheses for the dynamic model include (i) frictionless (reversible) motion of the parts modeled as (ii) rigid bodies (iii) undergoing plane **xy** motion at best; (iv) simple **y**-axis reciprocating *translation* for the piston; (v) simple *rotation* around the **z**-axis for the crank and flywheel (not shown); (vi) the piston center of mass is located in the **y**-axis; and (vii) the crank center of mass is at the reference coordinate system origin. Moreover, m_p and m_r are the piston and rod masses, respectively; I_r, I_f, and I_c are rod, flywheel, and crank inertias.

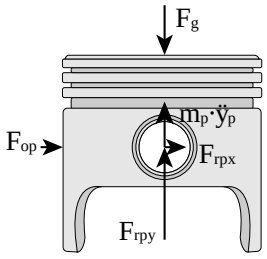

Figure 2. Free body diagram for the piston. Adapted from Tzortzinis (2015).

2.2.1 Kinematics

The two right-triangles with hypotenuses R and L of Fig. 1 play a key role in the dynamic model. Let $B \equiv R/L$, $\beta_x \equiv h/\ell = \tan\phi$, and $\beta_y \equiv r/\ell = \tan\phi/\tan\alpha$, one has:

$$\sin\phi = B\sin\alpha, \qquad \dot{\phi} = \beta_y\dot{\alpha} = \beta_y\omega, \qquad \ddot{\phi} = \begin{bmatrix}\mathsf{a}_\omega & \mathsf{a}_{\dot\omega}\end{bmatrix}\begin{bmatrix}\omega^2\\ \dot\omega\end{bmatrix} \equiv \mathbf{a}\boldsymbol{\Omega}, \qquad \text{with} \qquad \mathbf{a} = \begin{bmatrix}\beta_x(\beta_y^2-1) & \beta_y\end{bmatrix}. \tag{8}$$

Let $(\mathsf{x},\mathsf{y})_{p,r,c}$ be the **x**- and **y**- coordinates for the piston, rod and crank respective centers of mass. One has:

$$\ddot{\mathsf{y}}_p = \mathbf{y}_p\boldsymbol{\Omega}, \qquad \text{with} \qquad \mathbf{y}_p \equiv \begin{bmatrix}\mathsf{y}_{p\omega} & \mathsf{y}_{p\dot\omega}\end{bmatrix} = -\begin{bmatrix}r(1+\beta_y)+h\mathsf{a}_\omega & h(1+\beta_y)\end{bmatrix}, \tag{9}$$

$$\ddot{\mathsf{x}}_r = \mathbf{x}_r\boldsymbol{\Omega}, \qquad \text{with} \qquad \mathbf{x}_r \equiv \begin{bmatrix}\mathsf{x}_{r\omega} & \mathsf{x}_{r\dot\omega}\end{bmatrix} = +\begin{bmatrix}-h(1-r_g) & r(1-r_g)\end{bmatrix}, \qquad r_g \equiv L_g/L, \tag{10}$$

$$\ddot{\mathsf{y}}_r = \mathbf{y}_r\boldsymbol{\Omega}, \qquad \text{with} \qquad \mathbf{y}_r \equiv \begin{bmatrix}\mathsf{y}_{r\omega} & \mathsf{y}_{r\dot\omega}\end{bmatrix} = -\begin{bmatrix}r(1+r_g\beta_y)+hr_g\mathsf{a}_\omega & h(1+r_g\beta_y)\end{bmatrix}. \tag{11}$$

The **x**- and **y**- component accelerations of the crank center of mass are both trivially zero by the hypothesis (vii) above.

2.2.2 Kinetics

In this work, solid-body exchanged force indices refer to the *action* of the element indicated by the first index onto the one indicated by the second index; while a third index, if present, refers to a Cartesian direction component; for instance, F_{rpy}, shown on Fig. 2, is the **y**-component of the action force of the rod onto the piston. F_g is the force applied by the thermodynamic system gas onto the piston, obtained from the gas pressure and the piston area.

Figure 2 shows the FBD for the piston component. Since neither engine vibrations nor support reactions are the focus of the model, equilibrium of forces in the **x**-direction, although trivial, is neglected. Dynamic equilibrium of forces in the **y**-direction, assuming all solid contact and inertial positive forces pointing upward, except for F_g, provides the following equation for F_{rpy}, in which $\mathbf{y}_p$ is given by Eq. (9):

$$F_{rpy} = F_g + m_p\ddot{\mathsf{y}}_p = F_g + m_p\mathbf{y}_p\boldsymbol{\Omega}. \tag{12}$$

Figure 3 shows the FBD for the rod component. Equilibrium of forces in the **y**-direction yields:

$$F_{cry} = F_g + \begin{bmatrix}m_r & m_p\end{bmatrix}\begin{bmatrix}\mathsf{y}_{r\omega} & \mathsf{y}_{r\dot\omega}\\ \mathsf{y}_{p\omega} & \mathsf{y}_{p\dot\omega}\end{bmatrix}\begin{bmatrix}\omega^2\\ \dot\omega\end{bmatrix} \equiv F_g + \mathbf{m}_{rp}\mathbf{y}_{rp}\boldsymbol{\Omega}, \tag{13}$$

in which $\mathbf{y}_{rp}$ components are given in Eqs. (9) and (11). Equilibrium of forces in the **x**-direction provides the following functional relation between F_{prx} and F_{crx}: $F_{prx} = -F_{crx} + m_r\ddot{\mathsf{x}}_r$.

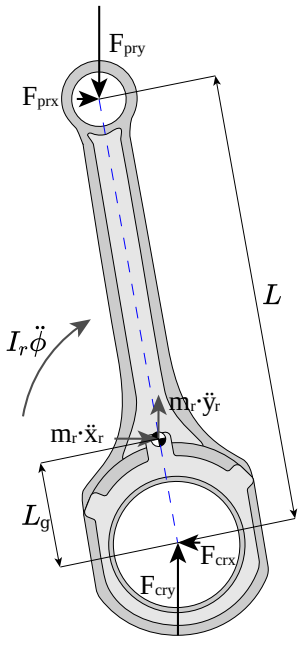

Figure 3. Free body diagram for the rod. Adapted from Tzortzinis (2015).

Equilibrium of force moments with respect to the rod center of mass provides the following:

$$F_{crx} = \frac{\mathbf{l}_{crx}\boldsymbol{\Omega} - hF_g}{\ell}, \quad \text{with} \quad \mathbf{l}_{crx} \equiv I_r\mathbf{a} - h\mathbf{m}_{rp}\mathbf{r}_{g1}\mathbf{y}_{rp} + \ell(1-r_g)m_r\mathbf{x}_r, \quad \text{and} \quad \mathbf{r}_{g1} \equiv \begin{bmatrix}r_g & 0\\ 0 & 1\end{bmatrix}, \tag{14}$$

where $r_g \equiv L_g/L$, shown in Fig. 3. Letting further $\mathbf{l}_{cry} \equiv \ell\mathbf{m}_{rp}\mathbf{y}_{rp}$, allows for $F_{cry} = F_g + \mathbf{l}_{cry}\boldsymbol{\Omega}/\ell$.

Now that the force exchange between rod and crank are determined, clockwise engine angular acceleration, $\dot{\omega}$, can be obtained from the equilibrium of force moments with respect to the engine axis, yielding:

$$\dot{\omega} = \frac{\mathsf{T}}{I_{\text{tot}}} = \frac{\mathsf{T}_s + \mathsf{T}_d}{\mathsf{I}_{pr\dot{\omega}} + I_c + I_f} = \frac{h(1+\beta_y)F_g - \mathsf{I}_{pr\omega}\omega^2}{\mathsf{I}_{pr\dot{\omega}} + I_c + I_f}, \tag{15}$$

in which T_s and T_d are static and dynamic (engine) torque components, respectively, which add up to T, the total instantaneous scalar engine torque, that is also positive in the clockwise direction. The line vector $\mathsf{I}_{pr} \equiv \begin{bmatrix}\mathsf{I}_{pr\omega} & \mathsf{I}_{pr\dot{\omega}}\end{bmatrix}$ is given by:

$$\mathsf{I}_{pr} = \left(\beta_y \mathsf{I}_{crx} - \beta_x \mathsf{I}_{cry}\right). \tag{16}$$

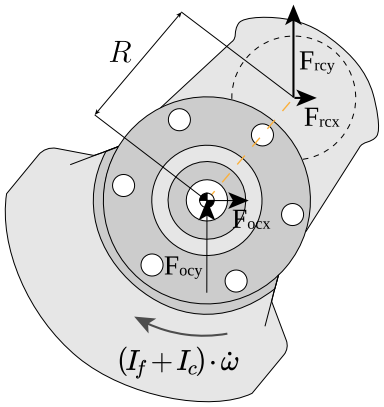

Figure 4. Free body diagram for the crank. Adapted from Tzortzinis (2015).

The instantaneous gas force at time t_i is given by $F_g = \mathsf{A}P_g$, where P_g is the net gas pressure and $\mathsf{A} = \pi D^2/4$ is the piston cross-section area.

Given engine design and operating parameters, as well as the thermodynamic state, Eq. (15) can be used in determining the instantaneous $\dot{\omega} \equiv \ddot{\alpha}$. The crankshaft angle variation $\Delta\alpha = \alpha_{i+1} - \alpha_i$ can be obtained by numerical integration of $\ddot{\alpha}$.

Our numerical code is implemented in the Julia language (Bezanson *et al.*, 2012)—a fast, dynamic, optionally typed, easy to use, and open-source language with many libraries (packages) for scientific computing.

The `DifferentialEquations.jl` Julia package (Rackauckas and Nie, 2017) is used to efficiently integrate Eq. (15) in the discrete time intervals. Since the pressure is also variable with α, we chose to use an average process pressure value with evacuated crank case for calculating F_g, meaning $P_g = (P_{i+1} + P_i)/2 - P_{cc}$, where P_{cc} is the crank case pressure.

3. VALIDATION

Five validation cases of (a) energy conservation with $q_{ent} = 0$ kJ/kg, (b) energy conservation with $F_g = 0$ kN, (c) classical ideal Otto cycle solution, (d) published FTHA cycle results (Naaktgeboren, 2017), and (e) purely dynamical total torque benchmark (Norton, 2010), were successfully run and documented for the two-way coupled model (Moreira, 2019). For briefness, only the first two validation cases are herein reported.

Model engine parameters for the validation tests are: $R = 37.00$ mm, $L = 120.78$ mm, $D = 89.00$ mm, $V_{min} = 550.00$ cm^3, $m_p = 0.417$ kg, $m_r = 0.287$ kg, $I_r = 6.63 \times 10^{-4}$ kg$\cdot$m^2, $I_f + I_c = 5.5$ kg$\cdot$m^2, and $P_{cc} = 0$ kPa. The working fluid is air and initial values are: $\alpha_0 = -\pi$ rad, $\omega_0 = 80\pi$ rad/s, $P_0 = 101.375$ kPa, $T_0 = 300$ K. Simulation time step was $\Delta t = 0.00002$ s $= 20$ µs.

3.1 Case of no thermal energy input

The validation case of no thermal energy input consists in setting $q_{ent} = 0$ kJ/kg for each cycle, while setting an initial engine speed—of 80π rad/s $= 2400$ RPM. Expected results are a succession of *identical* cycles due to the principle of conservation of energy—the first law of thermodynamics—since both dynamic and thermodynamic systems will *reversibly* absorb and release part of the initially available kinetic energy inventory into additional kinetic and internal energy forms.

Monitoring engine angular speed means monitoring flywheel and crank kinetic energy inventories. At the initial, BDC, condition, the thermodynamic system is at an internal energy minimum, and the piston is at a kinetic energy minimum. In the first mechanical cycle, the gas is reversibly compressed and expanded, thus causing a drop in engine angular velocity, as kinetic energy is reversibly converted to and from internal energy, as seen in the first half of Fig. 5.

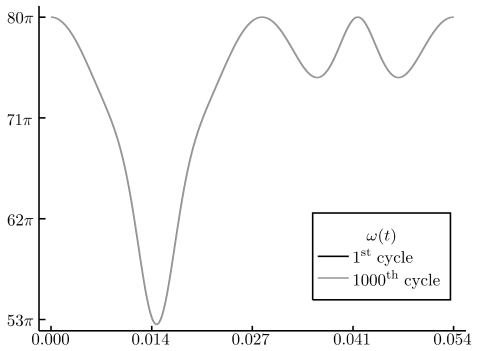

Figure 5. Crankshaft angular velocity history, in rad/s, for the first and one-thousandth thermal cycles for the no thermal energy input validation case. Coinciding (overlapping) values attest conservation of energy on the implemented model.

On the second half of Fig. 5—corresponding to the second mechanical cycle within the 4-stroke thermodynamic cycle—the gas pressure is kept constant so there's no internal energy storage, while the piston experiences velocity minima at either bottom and top DC's, and velocity maxima at some intermediate point. This causes engine angular velocity to experience local minima and maxima at twice the frequency of the first mechanical cycle. Fig. 5 results also display this qualitative agreement, and the quantitative one that every local ω maximum occurs with the exact same value of ω.

3.2 Case of no working fluid net pressure

The validation case of no working fluid pressure consists in steadily setting $F_g = 0$ kN, while setting an initial engine speed—of 80π rad/s $= 2400$ RPM. The experimental analog is to run a reversible, frictionless engine in a test rig without the cylinder head.

Expected results are a succession of *identical* cycles due to the principle of conservation of energy—the first law of thermodynamics—since the dynamic system will *reversibly* absorb and release part of the initially available kinetic energy inventory into additional kinetic energy form. Instead of presenting two distinct half thermal cycles, this validation case should produce two identical half thermal cycles, which is exactly what is shown in Fig. 6.

Validation is achieved not only by this qualitative match, but chiefly quantitatively, by the repetition of engine angular velocity maxima and minima values along 1000 thermal cycles.

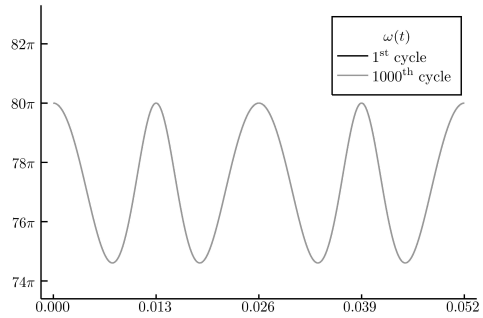

Figure 6. Crankshaft angular velocity history, in rad/s, for the first and one-thousandth thermal cycles for the no working fluid pressure validation case. Coinciding (overlapping) values attest conservation of energy on the implemented model.

4. RESULTS

4.1 Case of single cycle acceleration

Validated code results for model engine parameters of $R = 44.95$ mm, $L = 157.32$ mm, $D = 76.20$ mm, $V_{min} = 443.00$ cm^3, $m_p = 1.300$ kg, $m_r = 1.126$ kg, $I_r = 6.63 \times 10^{-4}$ kg$\cdot$m^2, $I_f + I_c = 100$ kg$\cdot$m^2, and $P_{cc} = 0$ kPa; working fluid is air, cycle $q_{ent} = 400.0$ kJ/kg, $\theta = -0.2618$ rad, $\Delta t_c = 4.0$ ms, and initial values of: $\alpha_0 = -\pi$ rad, variable 112.5 RPM $\leqslant \omega_0 \leqslant$ 7200 RPM in 64 linearly equally spaced cases with $P_0 = 101.375$ kPa, $T_0 = 300$ K, and simulation time step of $\Delta t = 0.0001$ s were obtained.

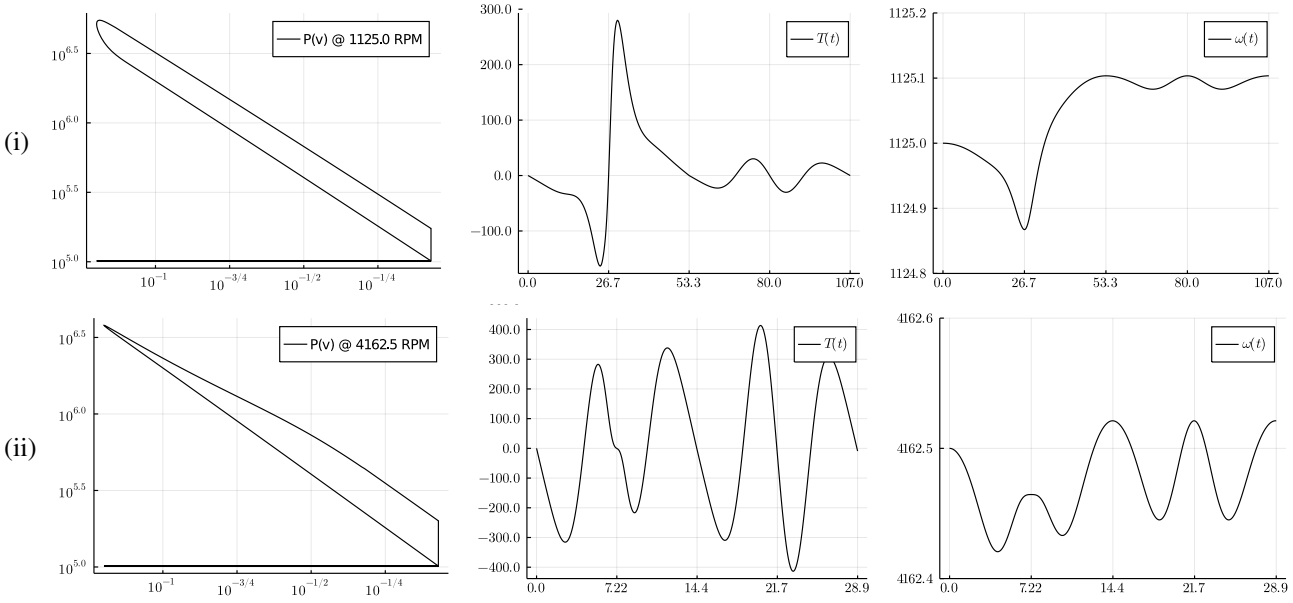

Figure 7. $(\log P \times \log v)$-cycle with P in Pa and v in m^3/kg (left column); instantaneous torque history, $\mathsf{T}(t)$, in Nm, (center column) and instantaneous angular velocity history, $\omega(t)$, in RPM, (right column) for the $\omega_0 = 1125$ RPM (top line) and $\omega_0 = 4162.5$ RPM (bottom line) cases.

Fig. 7 shows (a) thermodynamic cycles, in $(\log P \times \log v)$-coordinates in its leftmost column, (b) instantaneous torque histories, in its center column, and (c) instantaneous engine angular velocity histories, in the rightmost column, for two selected cases out of the 64 simulated ones, corresponding to (i) $\omega_0 = 1125$ RPM, in its topmost line, and (ii) $\omega_0 = 4162.5$ RPM, in its bottommost line.

Key thermal model characteristics include: (α) finite-time heat addition, with simultaneous heat and work interactions occurring at highest pressures and lowest specific volumes; (β) isochoric heat discharge at maximum specific volumes;

(γ) absence of pumping effects and resulting steady pressure on the exhaust and admission strokes. The effect of the dynamic model on the thermodynamic one is mostly seen by comparing results "a.i" with "a.ii", according to the labeling of the previous paragraph. At higher engine RPMs, heat being release at a fixed time interval Δt_c spans a wider crankshaft angular interval (and specific volume variation), which causes the process path to slowly approach the isentropic expansion quasi-straight[1] line during heat release. This effect is very evident in result "a.ii".

Moreover, the higher initial exhaust pressure shown in the "a.ii" subfigure of Fig. 7, if compared to that of the "a.i" subfigure, indicates a larger amount of heat being removed in the modeled exhaust process, and consequently, lower efficiencies at higher engine RPMs.

The key model characteristic of (δ) dynamic-thermodynamic coupling, allows for observation of thermally-driven operating regimes from dynamically-driven operating ones, as is the case when subfigures "b.i" and "b.ii" of Fig. 7 are compared. In lower RPMs, the model indicates a thermally-driven influence on instantaneous torque—since compression and expansion are the most predominant features. In higher RPMs, however, instantaneous torque fluctuations are predominantly due to dynamic effects.

There are other noteworthy between subfigures "b.i" and "b.ii" of Fig. 7. For lower RPMs, i.e., in the thermally-driven regime, instantaneous torque is consistent with the compression and expansion strokes, being consistently negative in the former, and consistently positive in the latter. At higher RPMs, however, in the dynamically-driven regime, one observes positive, useful work-producing torques at the final stages of the compression stroke and the opposite at the first stages of the expansion stroke, which can be deemed counter-intuitive!

At late stages of compression, the piston is in deceleration towards the TDC. Its inertia provides *more than enough* to compress the working gas, and positive instantaneous torques appears in the crankshaft. On the other hand, in early stages of expansion, piston inertia *requires a lot* to be accelerated towards the BDC; this fact coupled with comparatively slow heat addition and lower expansion stroke pressures that those occurring at lower RPMs, cause negative instantaneous torques to appear in the crankshaft.

Similar observations can be made based on the "c.i" and "c.ii" subfigures of Fig. 7. In the thermally-driven regime, the drop in engine instantaneous RPM is mostly due to the compression stroke, while the rise in engine instantaneous RPM is mostly due to the expansion stroke, as one can see from the "c.i" subfigure, in the top-right portion of Fig. 7. On the other hand, dynamic effects are prevalent in setting instantaneous engine RPMs variations along the cycle, as shown in the "c.ii" subfigure, in the bottom-right portion of Fig. 7.

In all cases, though, the cycle imposes a *net* increase in engine instantaneous angular velocity, as expected, so that such 'no-load, energy-input' cycle of the reversible engine causes it to end up at a higher angular speed than what it initially had. The coupling of the dynamic model thus allow the engine to perform work on itself, thus increasing its energy inventory (storage), which is in the kinetic form in its inertial solid parts. The net gain of engine instantaneous RPM between consecutive heat-input, no-load cycles *decreases* with the initial engine RPM, since kinetic energy is proportional to velocity squared, and, owing the the cycle analysis, a smaller thermal efficiency of the engine at higher RPMs.

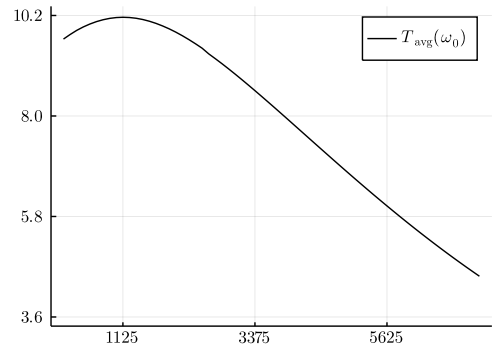

Figure 8. Cycle-averaged engine torque, in Nm, versus initial engine RPM for all 64 simulated cases with 112.5 RPM $\leqslant \omega_0 \leqslant 7200$ RPM.

Fig. 8 shows the cycle-averaged engine torque as a function of initial engine angular velocity, or, the engine torque curve. There is *some* curve shape resemblance to experimentally obtained torque curves, in the sense of having a generally negative second derivative—seen by the overall downward curve concavity—and a resulting global maximum torque value; however, one does not attempt in making further comparisons, as the test set kept all other parameters—chiefly q_{ent} and Δt_c—constant, which significantly differs from actual engine test and usage conditions.

The present model is, however, able to predict lower thermal efficiencies for higher engine speeds and constant Δt_c, as in (Naaktgeboren, 2017); and through the ω^2 component of $\mathbf{\Omega}$, from Eq. (8), significantly larger dynamic forces at higher engine angular velocities, which contribute to lower average torques at higher engine RPMs.

4.2 Case of multi-cycle acceleration

Validated code results for model engine parameters of $R = 37.0\,\mathrm{mm}$, $L = 120.78\,\mathrm{mm}$, $D = 89.0\,\mathrm{mm}$, $V_{min} = 550.00\,\mathrm{cm}^3$, $m_p = 0.417\,\mathrm{kg}$, $m_r = 0.283\,\mathrm{kg}$, $I_r = 6.63 \times 10^{-4}\,\mathrm{kg \cdot m}^2$, $I_f + I_c = 100.5\,\mathrm{kg \cdot m}^2$, and $P_{cc} = 0\,\mathrm{kPa}$; working fluid is air, cycle $q_{ent} = 600.0\,\mathrm{kJ/kg}$, $\theta = 0.0\,\mathrm{rad}$, $\Delta t_c = 1.0\,\mathrm{ms}$, and initial values of: $\alpha_0 = -\pi\,\mathrm{rad}$, $\omega_0 = 1000\,\mathrm{RPM}$, $P_0 = 101.375\,\mathrm{kPa}$, $T_0 = 300\,\mathrm{K}$, and simulation time step of $\Delta t = 1\,\mu\mathrm{s}$ were generated for multiple

[1] For constant working fluid specific heats, isentropic expansions display as straight lines in P-v log log diagrams.

consecutive cycles, in this heating-no-load condition, until the engine angular velocity reached or exceeded $4000\ \mathrm{RPM}$ by the end of a cycle—which took 45 cycles and a little over $2.1\ \mathrm{s}$ of operation. Owing to the small time step, the entire simulation ran for 2,116,429 iterations.

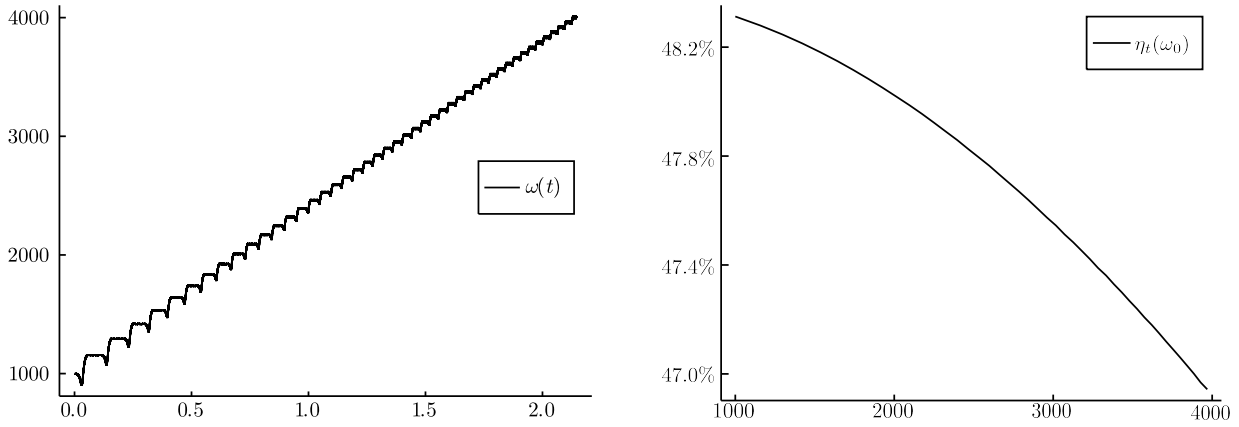

Figure 9. Angular velocity history, $\omega(t)$, (left) and thermal efficiency in terms of initial engine angular velocity, $\eta_t(\omega_0)$, (right).

Fig. 9 shows plots for $\omega(t)$, on the left, and for $\eta_t(\omega_0)$, on the right. Overall, thermal efficiencies are low for a reversible air-standard model, and the drop in thermal efficiency with respect to increased engine angular velocity is small. This is likely due to the relatively late ignition, occurring at the TDC for all cases, as $\theta = 0.0$, so roughly the same amount of energy was added to the engine system with each cycle, in the kinetic form, showed on Fig. 9 through increased engine angular velocity with time.

With increasing engine angular velocity, cycles become more frequent, and heat energy is added at increasing rates, i.e., at higher heat-powers, and so does the (equivalent) fuel consumption (not simulated in an air-standard model), and the rate of additional kinetic energy storage within the engine. During such a regime, cumulative energy storage is predominantly quadratic with time, which explains the predominantly linear increase of engine angular velocity with time on the left side of Fig. 9.

It is worth noting that the increase in engine angular velocity monotonically *decreases* with increasing ω_0, meaning that the "steps" seen on the left side of Fig. 9 become increasingly shallower, however, increasingly frequent as well.

5. CONCLUSIONS

Results have shown that a simple, two-way coupled, inertial, air-standard, internally reversible, finite-time heat addition Otto engine model is able to predict engine performance parameters such as instantaneous engine torque, angular velocity, as well as engine P-v diagram, thermal efficiency, and average torque curve—from which an engine power diagram can be derived.

As shown in the discussions, many energy transfer modes can be discussed and insights can be provoked by generating and analyzing model results. The model has a reasonably decent amount of input parameters, thus allowing for many case studies to be performed.

The model can thus serve as a teaching resource in advanced engineering classes, as well as a departure point for more complete equilibrium models that account for: valves and flow, combustion and chemical equilibrium, with heat-transfer and pressure-drop irreversibilities, on the thermodynamic "side", as well as progressively more detailed dynamic elements, such as more complex mechanisms and unbalanced elements, coupling and decoupling clutches, multiple gears, multi-cylinder engine, friction irreversibilities, and the like.

ACKNOWLEDGMENTS

The authors are thankful to the Universidade Tecnológica Federal do Paraná - UTFPR, Guarapuava Campus, for providing teaching, mentoring and research opportunities, as well as institutional access to bibliographic databases.

The authors glorify their Lord and God Jesus Christ, through whom all things came into being, in whom are hidden all the treasures of wisdom and knowledge, and in whom we have redemption, the forgiveness of sins.

REFERENCES

Barros, J.E.M., 2003. *Estudo de motores de combustão interna aplicando análise orientada a objetos*. Master's thesis, Universidade Federal de Minas Gerais.

Bezanson, J., Karpinski, S., Shah, V.B. and Edelman, A., 2012. "Julia: A fast dynamic language for technical computing". *Computing Research Repository*. doi:arXiv:1209.5145.

Borgnakke, C. and Sonntag, R.E., 2009. *Fundamentals of Thermodynamics*. Wiley, 7th edition.

Brunetti, F., 2012. *Motores de combustão interna*, Vol. Volume 1. Edgard Blücher Ltda. ISBN 9788521207085.

Curto-Risso, P.L., Medina, A. and Hernández, A.C., 2008. "Theoretical and simulated models for an irreversible otto cycle". *Journal of Applied Physics*, Vol. 104, pp. 094911–1–11. doi:http://dx.doi.org/10.1063/1.2986214.

de Souza Neves, G.F.G., 2010. *Análise cinemática, dinâmica de vibração e de tensão em motores de combustão interna com virabrequim e bielas flexíveis*. Master's thesis, Universidade Estadual de Campinas.

Ebrahimi, R., 2014. "Thermodynamic simulation of performance of an irreversible otto cycle with engine speed and variable specific heat ratio of working fluid". *Arab J Sci Eng*, Vol. 39, pp. 2091–2096. doi:10.1007/s13369-013-0769-9.

Hernandez, A.C., Medina, A., Roco, J.M.M. and Velasco, S., 1995. "On an irreversible air standard otto-cycle model". *European Journal of Physics*, Vol. 16, No. 2, pp. 73–75.

Horváth, P. and Égert, J., 2015. "Stress analysis and weight reduction of a one-cylinder engine crankshaft". *Acta Technica Jaurinensis*.

Huleihil, M., 2011. "Effects of pressure drops on the performance characteristics of air standard otto cycle". *Physics Research International*, Vol. 2011, No. 496057, pp. 1–7. doi:doi:10.1155/2011/496057. Article ID 496057.

Liley, P.E., 1999. "Maximum work output for gas cycles with constraint". *International Journal of Mechanical Engineering Education*, Vol. 27, No. 4, pp. 311–316. doi:10.7227/IJMEE.27.4.4.

Martins, J.J.G., 2013. *Motores de Combustão Interna*. Publindústria, Porto, 4th edition. In Portuguese.

Montazersadgh, F.H., 2007. *Stress analysis and optimization of crankshafts subject to dynamic loading*. Master's thesis, The University of Toledo.

Moreira, F.M., 2019. "Modelo de acoplamento dinâmico–termodinâmico padrão a ar de tempo finito de adição de calor de motor otto". URL `http://repositorio.roca.utfpr.edu.br/jspui/handle/1/11553`.

Mozurkewich, M. and Berry, R.S., 1982. "Optimal paths for thermodynamic systems: The ideal otto cycle". *Journal of Applied Physics*, Vol. 55, No. 1, pp. 34–42. doi:http://dx.doi.org/10.1063/1.329894.

Naaktgeboren, C., 2017. "An air-standard finite-time heat addition otto engine model". *International Journal of Mechanical Engineering Education*.

Naaktgeboren, C., 2020. "On exact and local polytropic processes: Etymology, modeling, and requisites". doi:10.31224/osf.io/ca6d4. URL `engrxiv.org/ca6d4`.

Norton, R.L., 2010. *Cinemática e dinâmica dos mecanismos*. Mc Graw Hill. ISBN 978-85-63308-19-1.

Özcan, H., 2011. "The effects of heat transfer on the exergy efficiency of an air-standard otto cycle". *Heat Mass Transfer*, Vol. 47, pp. 571–577. doi:10.1007/s00231-010-0749-5.

Rackauckas, C. and Nie, Q., 2017. "DifferentialEquations.jl – a performant and feature-rich ecosystem for solving differential equations in julia". *Journal of Open Research Software*, Vol. 5. doi:10.5334/jors.151.

Rubin, M.H., 1979. "Optimal configuration of a class of irreversible heat engines. i". *Phys. Rev. A*, Vol. 19, p. 1272. doi:http://dx.doi.org/10.1103/PhysRevA.19.1272.

Salamon, P. and Nitzan, A., 1981. "Finite time optimizations of a newton's law carnot cycle". *The Journal of Chemical Physics*, Vol. 74, No. 6, p. 3546. doi:http://dx.doi.org/10.1063/1.441482.

Seddak, M. and Liazid, A., 2017. "An experimental study on engine dynamics model based on indicated torque estimation". *Arab J Sci Eng*.

Tzortzinis, A., 2015. "piston-cranckshaft-connecting rod assembly". *GRABCAD*. URL `https://grabcad.com/library/piston-cranckshaft-connecting-rod-assembly-1`.

Villalva, S.G., 2014. *Análise de virabrequins automotivos utilizando modelos analíticos e flexíveis*. Master's thesis, Universidade Estadual de Campinas.

Çengel, Y.A. and Boles, M.A., 2013. *Termodinâmica*. AMGH, Porto Alegre. ISBN 978-85-8055-200-3.

RESPONSIBILITY NOTICE

The authors are solely responsible for the printed material included in this paper.